

Region-Specific Characterization of *N*-Glycans in the Striatum and Substantia Nigra of an Adult Rodent Brain

Juhi Samal, Radka Saldova, Pauline M. Rudd, Abhay Pandit, and Róisín O'Flaherty*

Cite This: *Anal. Chem.* 2020, 92, 12842–12851

Read Online

ACCESS |



Metrics & More

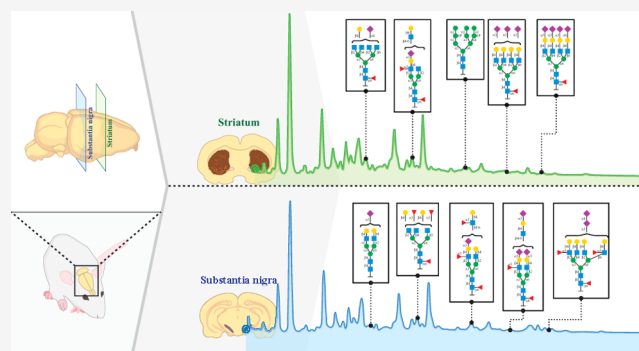


Article Recommendations



Supporting Information

ABSTRACT: *N*-glycan alterations in the nervous system can result in different neuropathological symptoms such as mental retardation, seizures, and epilepsy. Studies have reported the characterization of *N*-glycans in rodent brains, but there is a lack of spatial resolution as either the tissue samples were homogenized or specific proteins were selected for analysis of glycosylation. We hypothesize that region-specific resolution of *N*-glycans isolated from the striatum and substantia nigra (SN) can give an insight into the establishment and pathophysiological degeneration of neural circuitry in Parkinson's disease. Specific objectives of the study include isolation of *N*-glycans from the rat striatum and SN; reproducibility, resolution, and relative quantitation of *N*-glycome using ultra-performance liquid chromatography (UPLC), weak anion exchange-UPLC, and lectin histochemistry. The total *N*-glycomes from the striatum and SN were characterized using database mining (GlycoStore), exoglycosidase digestions, and liquid chromatography-mass spectrometry. It revealed significant differences in complex and oligomannose type *N*-glycans, sialylation (mono-, di-, and tetra-), fucosylation (tri-, core, and outer arm), and galactosylation (di-, tri-, and tetra-) between striatum and SN *N*-glycans with the detection of phosphorylated *N*-glycans in SN which were not detected in the striatum. This study presents the most comprehensive comparative analysis of relative abundances of *N*-glycans in the striatum and SN of rodent brains, serving as a foundation for identifying “brain-type” glycans as biomarkers or therapeutic targets and their modulation in neurodegenerative disorders.



The biological roles of glycans cover a broad spectrum of protective, organizational, and barrier functions making them crucial for the growth and survival of host organisms. *N*-Glycosylation is the most common type of post-translational modification in eukaryotic cells^{1,2} and involves the attachment and processing of oligosaccharide chains to some asparagine residues on proteins. Cell surface *N*-glycans are involved in several essential cellular functions including cellular and cell–matrix interactions. They also play crucial roles in cell adhesion, differentiation, synaptogenesis, and myelinogenesis during the development of the central nervous system (CNS).³

Early predictions for glycans mediating neural cell interactions in the developing and adult nervous system were based on the cell-specific complex gangliosides and cell-surface glycosyltransferases expressed by neural cells.^{4,5} Since then, the ubiquitous distribution of glycosylation in the CNS and its facilitation of functional processes that depend on cell recognition, such as migration, neurite outgrowth, synapse formation, and stabilization, has led to significant investigations of the biological implications for glycosylation in developmental processes^{6,7} and disease pathophysiology.⁸ The most notable role of *N*-glycans for the nervous system is highlighted by congenital glycosylation disorders,⁹ resulting in different neuropathological symptoms such as mental

retardation, seizures, and epilepsy. Examples of such congenital *N*-glycosylation disorders targeting the CNS include PMM2-CDG (CDG-Ia)^{10,11} and ALG6-CDG (CDG-Ic).¹¹

Thorough understanding of the identity and functional roles of glycans in the nervous system will provide us with a better perspective on the nervous system function.¹² Investigation of the variations in the glycosylation patterns of proteins at the cellular and matrix level as well as specific regions in the brain could lead to the identification of molecular targets for devising efficient therapeutic targets. We are particularly interested in the striatum and substantia nigra (SN) type *N*-glycans, two regions important in Parkinson's disease. Because the biosynthesis of *N*-glycans undergoes a stringent spatio-temporal regulation, we hypothesize that the region-specific resolution of *N*-glycans isolated in these regions could give us an insight into their roles in regulating striatal and nigral cues for establish-

Received: March 19, 2020

Accepted: August 18, 2020

Published: August 20, 2020



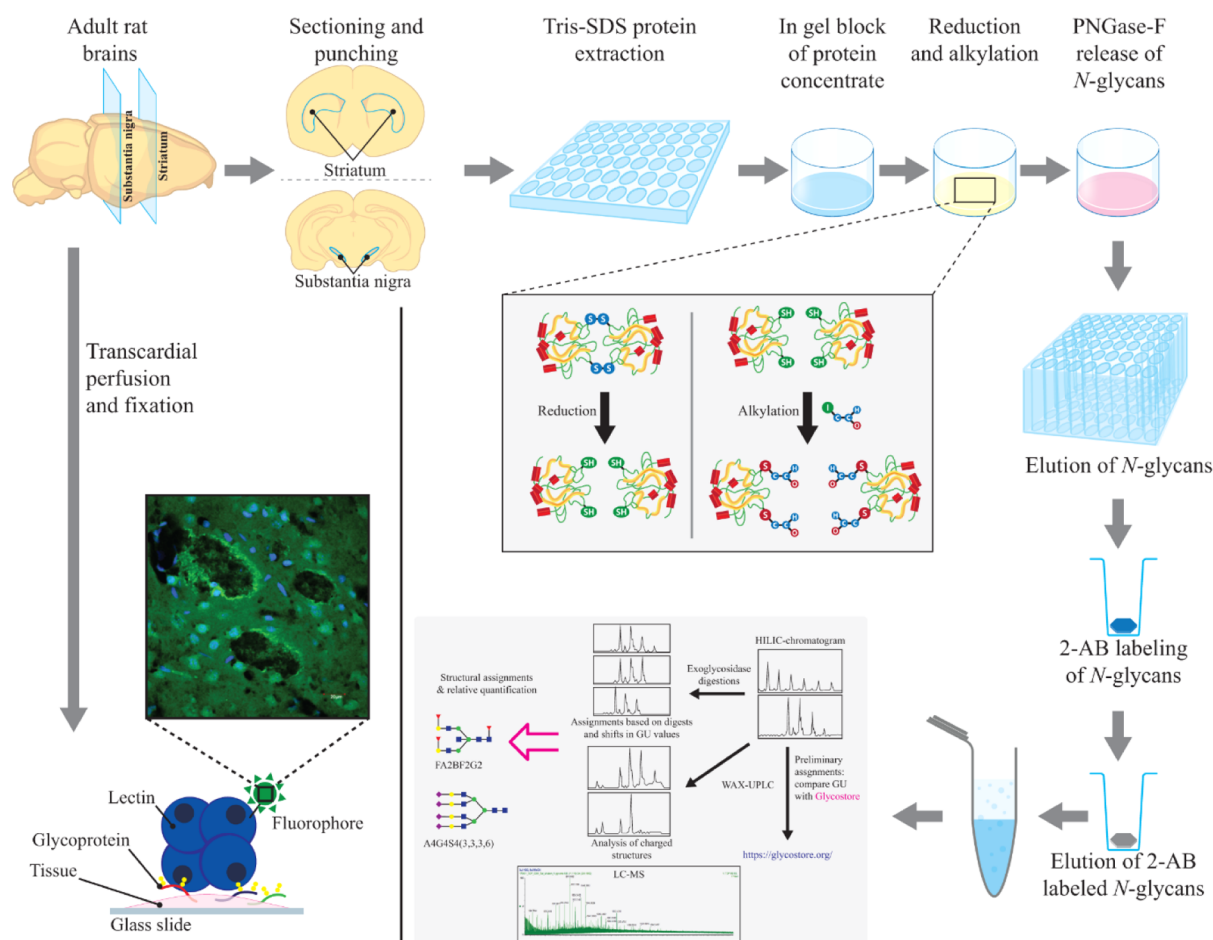


Figure 1. Schematic outline of the developed multifaceted glycoanalytical platform for the qualitative and quantitative analysis of rodent brain *N*-glycans for SN and striatum regions. The schematic outlines different stages of protein isolation and *N*-glycan isolation followed by different analytical techniques used to establish the platform including HILIC-UPLC, WAX-UPLC, GU values (<https://glycostore.org/>), exoglycosidase digestions and LC-MS. Lectin histochemical analyses were performed semiquantitatively to represent the changes in *N*-glycosylation over the two regions of the brain.

ment and pathophysiological degeneration of neural circuitry in Parkinson's disease. Future efforts by our team will test this hypothesis and probe how *N*-glycosylation is altered during the course of the disease. The detailed characterization provided in this manuscript will form the basis for these comparisons.

Previous studies have reported the conservation of *N*-glycan processing in rodent brains.^{13–15} The structural analyses performed to date have used *N*-glycan methodologies such as hydrazinolysis for *N*-glycan release, characterization of charged/neutral *N*-glycans separately (which limits the comparability of these glycans to each other), and/or the use of normal phase HPLC for separation of *N*-glycans.^{13,14} These studies, though very comprehensive for their time, have paved the way for more modern *N*-glycoanalytical approaches with higher resolution capabilities. In a different approach, Ji *et al.* performed a mouse brain *N*-glycan analysis where they used the glycans extracted from the plasma membranes of the tissue samples for downstream analysis.¹⁶ Another study has highlighted spatially specific regulation of *N*-glycans in different regions of the brains of healthy and glioblastoma mouse models using matrix-assisted laser desorption/ionization (MALDI)-MSI.¹⁷ These studies emphasize further the need for a detailed *in vivo* analysis for specific regions in the brain to elucidate further the correlation of glycosylation with the regulation of biological functions. Most importantly, the

resolution of striatum or SN glycan profiles has only been performed in a minimal capacity to date. Recently Raghunathan *et al.* presented an analysis of the differential *N*-glycome and proteome in the nigrostriatal space related to the age of the animals.¹⁸ Their broad analysis presents glycan compositions instead of *N*-glycan structures. This study provides ample grounds to support our working hypothesis and for further detailed investigation into the more detailed structure-specific glycan compositions in these regions of the brain.

In this study, we present a robust glycoanalytical technology to analyze the overall *N*-glycosylation of the rodent brain striatum and SN, two regions particularly relevant for Parkinson's disease. Using a combination of hydrophilic interaction chromatography (HILIC)–ultra-performance liquid chromatography (UPLC), electrospray ionization–mass spectrometry, weak anion-exchange chromatography (WAX)-UPLC, database mining (GlycoStore, <https://glycostore.org/>), exoglycosidase sequencing, and lectin histochemistry, we present a detailed comparative analysis of relative abundances of *N*-type glycans in the SN and striatum of adult rat brains. Analysis using this robust platform revealed region-specific modulation of *N*-glycosylation in the rodent brains, and this was correlated well to the regional cellular composition and their projected biological significance. To the

best of our knowledge, this is the most comprehensive platform for region-specific resolution of *N*-glycans in rodent brains to extensively characterize and compare their striatum and SN *N*-glycome. This is of particular relevance for future studies to probe the possible correlation of *N*-glycosylation and its modulation and function in the neurodegenerative disorders like Parkinson's disease involving these regions of the brain.

RESULTS AND DISCUSSION

A very small percentage (less than 5%) of the brain's dry weight is composed of carbohydrates. This represents a minuscule fraction when compared to over 80% from lipids and proteins.²⁵ This signifies a major limitation for development of glycoanalytical techniques focusing on the whole brain tissue as, in general, they suffer from low sensitivity and high noise levels because of signal suppression. This study represents a major initiative to develop a glycoanalytical platform for the assessment of the region-specific regulation of *N*-glycosylation occurring in the neural tissue. Here, we have characterized the total *N*-glycome including all of the major neutral and charged *N*-linked glycans expressed in the striatum and SN of the adult rat using a combination of HILIC-UPLC, GU values from GlycoStore (<https://glycostore.org/>), exoglycosidase sequencing, and liquid chromatography mass spectrometry (LC-MS) as represented in Figure 1 ultimately to probe a rodent Parkinsonian model in future research efforts.

In detail, microbiopsied tissues from rat brains (using the brain atlas) were processed using Tris-SDS extraction followed by in gel blotting (IGB). The basis of selection of the protein extraction method was the optimization performed using three extraction protocols using Tris-SDS buffer, radioimmunoprecipitation assay buffer, and proteinase K (Supporting Information Figure S1). The criteria for opting for this method of extraction were the higher yield of tissue *N*-glycans and the ability to produce glycan peaks that were easy to resolve, reproduce, and integrate. Many previous reports of brain glycosylation have used either the whole brain homogenates^{13,14} or surgically dissected regions of the brain.^{16,26} Microbiopsy of specific regions of the brain from the cryosectioned tissue facilitates an efficient collection of the relatively smaller regions of the brain such as SN for protein extraction. Higher specificity of the current technique allows for a more defined region-specific resolution of *N*-glycans than the tissue excision used in the previous studies.

Immobilization of the isolated glycoproteins in polyacrylamide gel pieces²¹ minimizes the concerns arising from the presence of contaminants in a sample by allowing efficacious removal of contaminants from buffers used for the denaturation, reduction, and alkylation of the glycoproteins. The next stage of this platform deals with the release of *N*-glycans from the immobilized glycoproteins.

The *N*-glycan moieties from the gel-entrapped proteins were cleaved off with the endoglycosidase peptide: *N*-glycosidase F (PNGase F). Preferential treatment with PNGase F is attributed to its broad specificity toward almost all *N*-glycans unless the core is modified with an α 1-3 fucose.^{27,28} This step is followed by labeling with 2-AB using reductive amination which in complex biological extracts like tissues might result in side-products and poor labeling efficiency. The immobilization maximizes the removal of byproducts and contaminants prior to and after glycan fluorescence labeling. Labeled glycans were then analyzed by HILIC-UPLC with fluorescence detection,

and the pooled samples were characterized using GU values, WAX-UPLC, LC-MS, and exoglycosidase digestion panels.

Protocol Verification and Reproducibility. For protocol verification, seven biological replicates from striatal and nigral *N*-glycans were prepared respectively using our developed IGB²¹ glycoanalytical approach for brain *N*-glycan extraction and analysis. *N*-glycans from both tissue types were then analyzed on a UPLC system equipped with the BEH HILIC glycan column and fluorescent detection.

A complete stack plot of the tissue *N*-glycoprofiles (UPLC chromatograms of released *N*-glycans) is shown in Figure S2a and is indicative of reproducibility of the protocol optimized for *N*-glycan isolation from brain tissues. Seven biological replicates for each tissue type were run using the developed technology and visualized on HILIC-UPLC. The chromatograms obtained using HILIC-UPLC showed 26 integratable peaks for both striatum and SN, respectively (GP1-GP26). The coefficients of variation (C_v) between the samples for both tissue types were below 10% for all major peaks, that is, those peaks with a relative percentage area above 5% (Figure S2b,c). Only one peak was above 20% of variance in striatum, and two peaks showed values of variance above 20% in SN. Higher coefficients of variance ($C_v > 20\%$) were biased toward the small peaks at the beginning and end of the profile of very low intensity. Individual peak areas for both striatum and SN for all biological replicates are presented in Table S1, and the total directory of structures identified is presented in Table S2.

Region-Specific Regulation of *N*-Glycosylation. To the best of our knowledge, this is the most comprehensive analysis of the differential tissue *N*-glycosylation in SN and striatum regions of the brain. It holds great significance particularly in terms of investigating glycan-based biomarkers and their modulation in the disease pathophysiology for neurodegenerative disorders like Parkinson's disease, where these regions of the brain are chiefly implicated.

Representative UPLC chromatograms from the striatum and SN along with the corresponding major peak assignments in the 26 glycan peaks are presented in Figure S3 and Table S3. As a general trend, the first glycan species to be eluted as represented in the chromatograms are smaller neutral glycans, followed by larger sialylated and highly fucosylated charged glycans. Combined with LC-MS detection, HILIC-UPLC enabled simultaneous observation and quantification of both high- and low-abundance *N*-glycans. In our study, this multifaceted analysis with a series of exoglycosidase digestions enabled the detection of over 170 *N*-glycan isomers for both striatum and SN, originating from over 100 distinct *N*-glycan compositions. A representative digestion using the panel of enzymes used for the analysis is shown in Figure S4. The most abundant glycans in both striatum and SN were oligomannose or fucosylated complex type, though varying amounts of glycans were detected from all biosynthetic classes.

Specific differences between *N*-glycans characterized (by LC-MS and exoglycosidase panel) in this study for striatum and SN were localized to glycan peaks GP14, 18, 22, 24, and 26 in the HILIC-UPLC chromatograms, and in other glycan peaks, the same structures were detected. These glycan species are highlighted in Table S4 and the LC-MS spectra (detailed in Table S5) in Figure S5. As such, subtle variations in glycosylation features are evident between SN and substantia, and these regional alterations include fucosylation, sialylation, and mannosylation (Table S6 for more details on traits). The relative proportion of each UPLC glycan peak between the two

regions of interest was also measured. Statistically significant differences between striatum ($n = 7$) and SN ($n = 7$) in glycan peaks GP8 ($p < 0.001$), GP11 ($p < 0.05$), and GP13 ($p < 0.001$) were observed (Table S7). GP8 (striatum: 9.73%, SN: 10.98%) and GP13 (striatum: 7.32%, SN: 8.89%) were significantly higher while GP11 (striatum: 3.30%, SN: 3.98%) was lower in SN compared to the striatum (Figure S2b). For both brain regions, glycan peaks GP8 and GP13 contain oligomannose *N*-glycans M6 and M7, respectively, as major structures, whereas GP11 contains a triantennary difucosylated monogalactosylated structure (FA3F1G1) as the major structure (Table S3). Taken together, these results suggest that mannosylation expression may be differentially regulated in these regions of the brain (significant higher levels detected in SN).

Experimental Procedures. Chemicals and Reagents. All chemicals and proteins were purchased from commercial suppliers and used without any purification unless otherwise specified. No unexpected or unusually high safety concerns were encountered in this research. Formic acid (FA) and Tris were obtained from AnalaR, VWR. Sodium bicarbonate (NaHCO_3) and ammonium bicarbonate (NH_4HCO_3) were obtained from HiPerSolv, BDH. ProtoGel was purchased from National Diagnostics, Hesse, Hull, UK. Ammonium persulfate was purchased from AnalaR; BDH and *N,N,N',N'*-tetramethylethane-1,2-diamine were obtained from Sigma-Aldrich. Iodoacetamide and dithiothreitol were obtained from Sigma-Aldrich. Sodium dodecyl sulfate (SDS), acetonitrile, and sucrose were obtained from Sigma-Aldrich. Ultrapure water was obtained from arium pro UV (Sartorius Stedim). 2-Aminobenzamide (2-AB) labeling of *N*-glycans was performed using a fluorescent labeling mix [50 μL , 350 mM 2-AB (Sigma), 1 M sodium cyanoborohydride (Sigma) in acetic acid (Sigma)/dimethyl sulfoxide (Sigma) (30:70)].¹⁹

Animals. Female Sprague-Dawley rats (Charles River, U.K.) were used in this study ($n = 35$), weighing 225–250 g at the start of the experiment. Animals were housed in groups of four per cage, on a 12:12 h light/dark cycle, at 19–23 °C, with the humidity level of the room maintained between 40 and 70% and with food and water being available *ad libitum* throughout the course of the experiment.

All procedures were carried out in accordance with the European Union Directive 2010/73/EU and S.I. no. 543 of 2012 and were completed under CAA license (B100/3827) issued to Dr. Eilís Dowd by the Irish Department of Health and Children and were reviewed and approved by The Animal Care and Research Ethics Committee of the National University of Ireland, Galway.

Perfusion. Rats were deeply anesthetized with pentobarbital (1 mL/kg) and transcardially perfused with 100 mL of ice-cold heparinized saline (5000 U/L) followed by 150 mL of 4% paraformaldehyde (pH 7.4). Their brains were removed and placed into 4% paraformaldehyde overnight for postfixation prior to transfer to 30% sucrose. After 48 h equilibration in sucrose solution, 30 μm serial sections of the fixed brains were cut using a freezing sledge microtome, and lectin staining was performed.

Tissue Homogenization. Tissue homogenates for *N*-glycan isolation and profiling were obtained by using Tris-SDS lysis buffer.²⁰ Briefly, collected tissue samples were resuspended in Tris-SDS lysis buffer (62.5 mM Tris pH 6.6, 2% SDS) for 20 min on ice followed by aspiration thrice and a further 20 min incubation. This was followed by homogenization using an

automated bead homogenizer (Qiagen TissueLyser LT) for complete lysis (40 Hz, 6 min). The supernatant was collected after centrifugation at 16,860 g for 20 min at 4 °C and dried overnight under vacuum centrifugation. The protein concentration in the samples was estimated using bicinchoninic acid (BCA) protein assay (Pierce BCA Protein Assay Kit, Thermo Fisher Scientific).

Release of *N*-Glycans from Striatal and Nigral Tissue Homogenates. *N*-glycans were released from dried tissue samples using the high-throughput method described by Royle *et al.*²¹ with a slight modification. Briefly, samples were immobilized in SDS-gel blocks to minimize the sample loss during transfer, reduced and alkylated in 96-well plates, and then washed. The *N*-linked glycans were released using peptide *N*-glycanase F (5 U of 100 mU/mL, NEB), as previously described.²²

2-AB Labeling of *N*-Glycans. *N*-glycans were fluorescently labeled with 2-AB by reductive amination.²³ Briefly, 2-AB labeling mixture was added to the released glycans, followed by agitation for 5 min to ensure proper mixing. This was followed by an incubation at 65 °C for 30 and 5 min agitation. The samples were then incubated at 65 °C for 1.5 h. The excess 2-AB reagent was removed on Whatman 3MM paper (Clifton, NJ) with acetonitrile, and the final elution of glycans was performed in water.^{19,20}

Ultra-performance Liquid Chromatography. UPLC was performed using BEH Glycan 1.7 μm particles in a 2.1 \times 150 mm column (Waters, Milford, MA) on an ACQUITY UPLC (Waters) equipped with a Waters temperature control module and a Waters ACQUITY fluorescence detector. Solvent A was 50 mM FA adjusted to pH 4.4 with ammonia solution. Solvent B was acetonitrile. The column temperature was set to 40 °C. A 30 min method was used with a linear gradient of 30–47% with buffer A at 0.56 mL/min flow rate for 23 min followed by 47–70% A and then to 30% A. Samples were injected in 70% acetonitrile. Fluorescence detection was performed using $\lambda_{\text{excitation}}$: 320 nm and $\lambda_{\text{emission}}$: 420 nm. The system was calibrated using an external standard of hydrolyzed and 2-AB labeled glucose oligomers to create a dextran ladder, as described previously.²⁰

Weak Anion-Exchange-(UPLC). WAX-HPLC was performed using a 10 μm BioSuite (diethylamino)ethyl (7.5 mm \times 75 mm) column (Waters) on a 2795 Alliance separation module with a Waters 2475 fluorescence detector ($\lambda_{\text{excitation}}$: 330 nm, $\lambda_{\text{emission}}$: 420 nm) as previously reported by Saldo *et al.*²⁴ Solvent A was 20% MeCN, and solvent B was 25 mM ammonium acetate buffer adjusted to pH 7.0. A linear gradient of 100% A to 100% B over 50 min at a flow rate of 0.75 mL/min was used. Samples were dissolved in water for this analysis. α -fetuin *N*-glycan standard was used for calibration.

Exoglycosidase Digestion. Samples from 18 animals were pooled for both striatum and SN, and a half was used for this analysis. All enzymes were purchased from ProZyme (San Leandro, CA, USA) or New England Biolabs (Ipswich, MA, USA). The 2-AB labeled glycans were digested in a volume of 10 μL for 18 h at 37 °C in 50 mM sodium acetate buffer, pH 5.5, using arrays of the following enzymes: *Arthrobacter ureafaciens* sialidase (ProZyme, 0.5 U/mL); bovine testes β -galactosidase (ProZyme, 1 U/mL); α 2-3 neuraminidase S (NAN1, NEB, 800 U/mL); bovine kidney α -fucosidase (ProZyme, 1 U/mL); β -*N*-acetylglucosaminidase cloned from *Streptococcus pneumoniae*, expressed in *Escherichia coli* (GUH, NEB, 800 U/mL and ProZyme, 8 U/mL); coffee bean α -

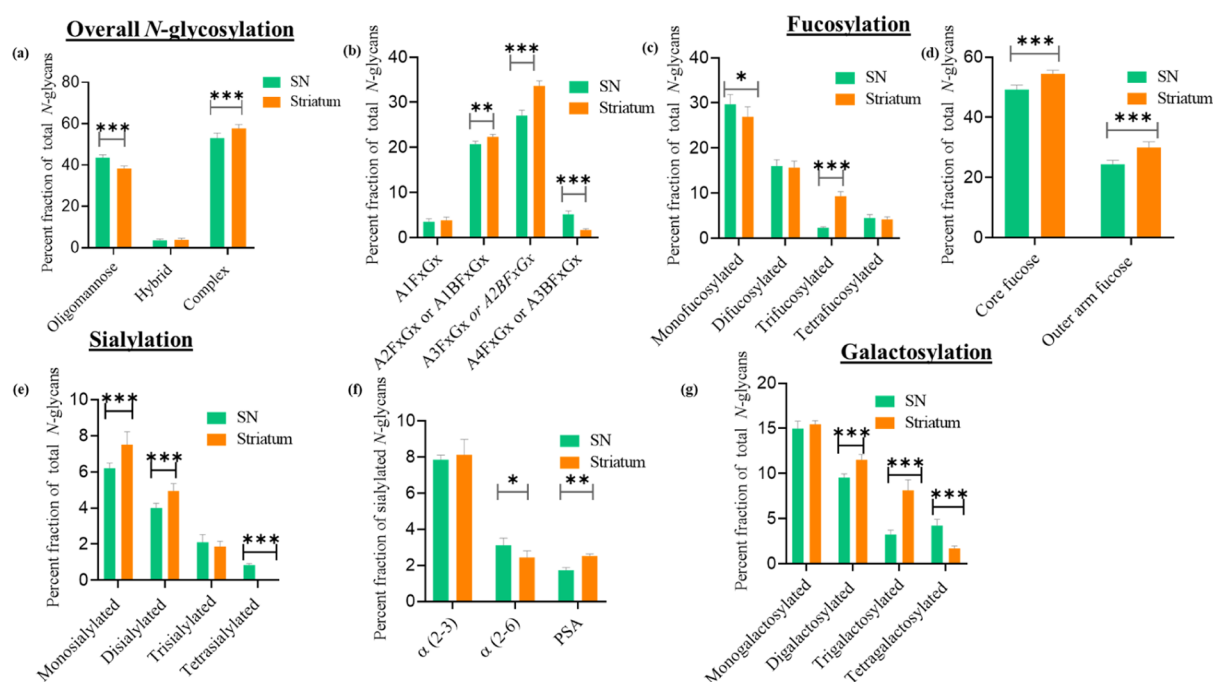


Figure 2. Relative regional abundances of total *N*-glycans. (a) Classification of the total *N*-glycans belonging to each of the three biosynthetic classes: oligomannose, complex, and hybrid in the striatum and SN of the rat brain indicating a region-specific distribution of *N*-glycosylation. (b) Classification of total *N*-glycans based on their antennary distribution (including bisecting GlcNAcs) in the striatum and SN in rat brains indicating higher levels of higher order tetra-antennary species and corresponding lower levels of lower order antennary species (di and tri-antennary) in SN. (c) Classification of fucosylated *N*-glycans according to degree of fucosylation (mono-, di-, tri-, and tetra-fucosylated) which includes both sialylated and asialylated fucosylated glycans. Tri-fucosylated species shows the largest difference in relative abundance. (d) Fucosylated *N*-glycans in striatum and SN of the rat brain differentiated by core and outer arm fucosylation indicating a distinct distribution between the two regions. (e) Classification of sialylated *N*-glycans according to the degree of sialylation (mono-, di-, tri-, and tetra-sialylated) in the striatum and SN of the rat brain. (f) Classification of sialylated *N*-glycans according to the sialic acid linkage type with the most notable effect with respect to polysialylation between regions. (g) Classification of galactosylated *N*-glycans. Most notable difference in di-galactosylated species between the SN and striatum. The trends are presented as mean \pm SD for $n = 7$ for each region, and the data were analyzed using two-way ANOVA with Bonferroni's post-hoc analysis with significance denoted as * $p < 0.05$, ** $p < 0.01$ and *** $p < 0.001$, respectively. The raw values are presented in Table S1, and p values are presented in Table S7.

galactosidase (NEB, 800 U/mL); and almond meal α -fucosidase (ProZyme, 0.4 mU/mL). After incubation, enzymes were removed by filtration through 10 kDa protein-binding E.Z. filters (Pall Nanosep 10K Omega). *N*-glycans were then analyzed by UPLC.

Liquid Chromatography-Mass Spectrometry. Samples from 18 animals were pooled for both striatum and SN, and a half was used for this analysis. Online coupled fluorescence-mass spectrometry detection was performed using a Waters Xevo G2 QToF with ACQUITY UPLC (Waters Corporation, Milford, MA, USA, 1 ppm resolution) and BEH Glycan column (1.0 \times 150 mm, 1.7 μ m particle size) as previously described by Saldova *et al.*²⁴ The instrument was operated in the negative-sensitivity mode with a capillary voltage of 1.8 kV for data acquisition. The ion source block and nitrogen desolvation gas temperatures were set at 120 and 400 $^{\circ}$ C, respectively. The desolvation gas was set to a flow rate of 600 L/h. The cone voltage was maintained at 50 V. The m/z range for full-scan data acquisition for glycans was in the range of 450–2500. The fluorescence detector settings were as follows: $\lambda_{\text{excitation}}$: 320 nm, $\lambda_{\text{emission}}$: 420 nm, and the data rate was 1 pts/s and a PMT gain = 10. The sample was injected at a volume of 10 μ L (75% MeCN) at 0.150 mL/min, and column temperature was maintained at 60 $^{\circ}$ C; solvent A was 50 mM ammonium formate (pH 4.4), and solvent B was MeCN. The linear solvent gradient over a span of 40 min was 28% A for 1

min, 28–43% A for 30 min, 43–70% A for 1 min, 70% A for 3 min, 70–28% solvent A for 1 min, and 28% A for 4 min. To avoid contamination of the system, the flow was sent to waste for the first 1.2 min and after 32 min. MassLynx 4.1 software (Waters Corporation, Milford, MA, USA) was used for data collection and processing.

Lectin Histochemistry. Brains were dissected out, and postfixation was performed for 4 h at room temperature. They were then transferred to 25% sucrose in phosphate buffer. For lectin histochemistry, slides were washed with Tris-buffered saline supplemented with Ca^{2+} and Mg^{2+} (TBS; 20 mM Tris-HCl, 100 mM NaCl, 1 mM CaCl_2 , and 1 mM MgCl_2 , pH 7.2) with 0.05% Triton X-100 (TBS-T) and then blocked with 2% periodate-treated bovine serum albumin (Sigma-Aldrich) in TBS for 1 h. All washes were three times for 5 min each, and all steps were performed at room temperature in a humidity chamber unless otherwise stated. Sections were washed then incubated with three different [*Anguilla anguilla* lectin (AAA) (15 μ g/mL), concanavalin A (Con A) (10 μ g/mL) and wheat germ agglutinin (WGA) (15 μ g/mL)] fluorescein isothiocyanate-conjugated lectins (EY Laboratories Inc.) in TBS for 1 h. Haptenic controls were carried out in parallel to verify lectin binding specificity by pre- (for 1 h) and co-incubating lectins in 100 mM of the appropriate haptenic sugar in TBS. Sections were washed five times with TBS-T and counterstained with 4',6-diamidino-2-phenylindole dihydrochloride (DAPI) for 20

min. The slides were washed in TBS-T before mounting the coverslip with ProLong Gold antifade (Life Technologies). Samples from each biological replicate ($n = 5$) were imaged using an inverted epifluorescence microscope (Olympus IX81, Olympus, Tokyo, Japan). Seven to nine images per section of each sample were taken at 20 \times magnification.

Glycosylation Features. The most abundant glycan constituents of each peak in the UPLC chromatogram based on exoglycosidase digestions were considered the representative feature for that peak (Figure S3). The glycosylation features were calculated by summation of the relevant dominant species in each glycan peak for a glycan trait, and these are presented in detail in Table S6. The inherent limitation of such analysis is the inability to include the features detected in trace amounts. We reported such features based on the combined knowledge from exoglycosidase analysis and mass spectrometry. This allows for more conclusive structural prediction as compared to the mass spectrometric analysis alone. The chief glycosylation features presented in this table include *N*-glycan type (oligomannose, complex and hybrid), charge analysis (including sialylation), galactosylation, fucosylation, and branching for both the striatum and SN. A major fraction of detected *N*-glycans for both the striatum and SN was the complex type glycans (striatum: 57.70%, SN: 53.03%). These included both asialylated and sialylated glycans and were followed in predominance by the oligomannose type (striatum: 38.44%, SN: 43.55%) and hybrid type (striatum: 3.86%, SN: 3.56%). Overall *N*-glycosylation traits are presented schematically in Figure 2a, and statistically significant peaks are highlighted (p values summary in Table S7). Region-specific regulation of *N*-glycosylation can be clearly observed in the distribution of these major structural classes of *N*-glycans in both tissue types where oligomannose structures are found in higher proportions (striatum: 38.44%, SN: 43.55%, $p < 0.001$) in SN and corresponding complex structures in lower proportions (striatum: 57.70%, SN: 53.03%, $p < 0.001$) relative to the striatum. This is in agreement with the findings from the individual glycan peak analysis. This reinforces the possibility of functional correlation of the glycosylation cues in different regions of the brain. Spatial resolution of glycans has previously been investigated in a few studies where the resolved glycans are used as a marker for disease progression²⁹ or to identify specific regions in a tissue.³⁰

Mannosylation. Oligomannose glycans are generally found in abundance among the neural *N*-glycans across different species. Previous studies have shown the significance of the cell surface expression of these glycans and its implications in neural tissue development.³¹ As already clarified, a distinctive regional regulation of oligomannose glycans was observed in the current study where a higher proportion of SN *N*-glycans (striatum: 38.44%, SN: 43.55%, $p < 0.001$) was observed to be mannosylated compared to the striatum, the biological relevance of which is yet to be discovered. Another significant feature detected in our study that has not been reported in any broad-spectrum analysis of brain *N*-glycans to date is the presence of mannose-6-phosphorylation (Man 6-P) of the oligomannose *N*-glycans (2.99%, Table S6). Interestingly, this feature was only detected in the SN glycans and was not confirmed as a major glycosylation feature in the striatum. A previous study conducted by Ji *et al.*¹⁶ in the mouse hippocampus reveals the specific absence of this feature in the hippocampus reinforcing the spatial regulation of

glycosylation. This post-translational modification is correlated with the intracellular transport of soluble lysosomal enzymes. The majority of the Man 6-P glycoproteins has been found to be localized in the neuronal lysosomes which appear to be a brain-specific feature as Man 6-P lysosomal enzymes showed endosome-like localization in the liver.³² SN has been shown to have a high activity level for most lysosomal enzymes in the previous studies,³³ and this correlates well with the detection of Man 6-P as a chief glycosylation trait for *N*-glycans isolated from SN. However, it is also possible that because tissues were homogenized for this analysis, the structures detected could include immature *N*-glycans from the golgi complex or endoplasmic reticulum. To this end, further investigation would be needed to confirm the subcellular localization and origin of these glycans in the tissue.

Branching and Bisecting GlcNAcs. In our structural characterization in this study, we were unable to unambiguously differentiate between biantennary structures and monoantennary structures with a bisecting GlcNAc (termed a bisect). This trend was repeated for all branching motifs. In terms of antennary distribution, there was an overall abundance of bi- and triantennary structures (or their bisect equivalents) when compared to mono- and tetra-antennary (or their bisect equivalents) *N*-glycans for the SN and striatum (Table S6). As represented in Figure 2b, there is a distinct regulation of the bi-, tri- and tetra-antennary glycans (or their bisects) between the striatum and SN which includes both the neutral and charged species. Most notably, there was a higher incidence of the bi-(striatum: 22.36%, SN: 20.74%, $p < 0.001$) and tri-antennary (striatum: 33.64%, SN: 27.06%, $p < 0.001$) glycans (or their bisects) in the striatum and lower levels of tetra-antennary (striatum: 1.70%, SN: 5.23%, $p < 0.001$) glycans (or their bisects) compared to SN. Bisecting GlcNAcs are known as general suppressors of terminal modifications of *N*-glycans,³⁴ but their specific role in brain biochemistry is yet to be fully explored and understood. A seminal study by Fogli *et al.*³⁵ elucidated the presence of bi- and triantennary (or their bisects) structures in the developmental brain disorders which highlight the significance of these antennary glycans as biomarkers for the developmental brain disorders.

Fucosylation. A wide distribution of fucosylated *N*-glycans has been observed in mammalian tissues especially the brain.³⁶ Two major *N*-glycan structures found abundantly in neural tissues by Shimizu *et al.* were both fucosylated and showed region-specific regulation in their distribution across different regions of the brain. Interestingly, these structures were not detected in the glycans isolated from the blood. This reinforces the biological significance of the fucosylated glycans in regulating the neural functions. Another study by Ji *et al.*¹⁶ investigating the spatial resolution of *N*-glycans in the mouse brain using a combination of tissue glyco-capture and nano-LC-MS further supports extensive fucosylation in the mouse brain (up to 55%, almost 30% of which are multiple fucosylated). Earlier investigations of *N*-glycome from serum or other tissues^{37,38} in mouse did not reveal such high levels of fucosylation which could be indicative of it being a typical "brain trait". A study by Eshghi *et al.*³⁹ analyzed the brain section from C57BL6 mice with MALDI-QIT-MS where they reported 42 *N*-linked glycans, 30 (71.4%) of which were fucosylated and 7 (16.7%) of which were nonfucosylated complex glycans. In our study, the proportions of fucosylated (both core and outer arm species) *N*-glycans in the striatum (56.13%) and SN (52.57%) are lower (Table S6). This is in

close agreement with the values for the mouse brain as investigated previously by Ji *et al.*¹⁶

In our study, fucosylated *N*-glycans from both tissue types were further classified on the basis of the degree of fucosylation, and a difference in distribution of differentially fucosylated species was identified (Figure 2c). As represented in Figure 2c (*p* values in Table S7), relatively high abundances of multiple-fucose (up to four fucose residues)-substituted *N*-glycans were detected in the striatum and SN with significant differences observed for the monofucosylated (striatum: 26.92%, SN: 29.67, *p* < 0.001) and trifucosylated (striatum: 9.36%, SN: 2.36%, *p* < 0.001) classes. Also, the differences in core fucosylated (striatum: 54.54%, SN: 49.29%, *p* < 0.001) and outer arm fucosylated (striatum: 30.02%, SN: 24.45%, *p* < 0.001) species were significant between the striatum and SN as represented in Figure 2d with the overall higher levels of fucosylation observed in the striatum. As previously reported by Chen *et al.*,¹⁴ a characterization study of rodent brain *N*-glycans (not region-specific), hybrid structures with outer arm $\alpha(1,3)$ - and core $\alpha(1,3)$ -fucosylation were detected in our study for both striatum and SN regions. However, outer arm fucosylated hybrids without core fucosylation were not detected in our hands. This is, therefore, anticipated to be a region specific characteristic not detected in the striatum or SN but in other regions of the brain.

The improved retention of a learned behavior in rats induced by intracerebral injection of fucose itself⁴⁰ points to the assumed link between alterations in the fucosylation of brain glycoproteins and mechanisms involved in memory storage. The enhanced enrichment of fucosylated species in striatal *N*-glycans could be associated with its involvement in stimulus-response learning. Aberrant fucosylation of the neural glycoproteins attributed to the absence of $\alpha(1,6)$ -fucosyltransferase is also known to result in the development of a schizophrenia-like phenotype in mice.⁴¹ This highlights the significance of fucosylation of glycoproteins in regulating their biological functions and hence augments the concept of differential regional regulation.

Sialylation. Sialylation is one of the most important forms of glycosylation in the CNS where it exists chiefly in the form of glycolipids,⁴² acting as receptors for toxins and pathogens⁴³ and mediating intercellular interactions through neural cell adhesion molecules (NCAMs).⁴⁴ There have been several studies that demonstrate the role of sialic acid-containing glycoconjugates in the differentiation and migration of neurons and axonal guidance.^{45,46} Dietary supplementation of sialic acid leads to increases in sialic acid-containing glycoproteins in the frontal cortex and is reported to accelerate learning and memory in piglets.⁴⁷ Alterations in the sialome of neuronal glycoproteins translate into their structural and functional aspects as reflected by sialic acid removal from membrane proteins in primary neurons leading to actin depolymerization and axonal growth.⁴⁸ In our study, HILIC-UPLC analysis of the *N*-glycans extracted from the striatum and SN revealed that a major proportion of isolated glycans were neutral (striatum: 85.68%, SN: 83.99%, *p* < 0.01) as represented in Tables S6 and S7). The degree of sialylation is presented in Figure 2e. From this analysis, we observed that the *N*-glycans isolated from SN show a lower overall sialylation when compared to the striatum (striatum: 14.32%, SN: 13.16%, *p* < 0.001). When comparing the degree of sialylation, statistically significant differences are observed for the monosialylated (striatum: 7.51%, SN: 6.20%, *p* < 0.001), disialylated (striatum: 4.95%, SN: 4.00%, *p* <

0.001), and tetrasialylated *N*-glycans (striatum: 0.84%, SN: 0%, *p* < 0.001). The overall trends aligned closely with the results from WAX analysis where the striatum showed higher levels overall with statistically significant differences in monosialylated and trisialylated *N*-glycans (Figure S6). In terms of the Neu5Ac-linked sialic acids, our study was in agreement with the previous studies investigating the charged *N*-glycans in rodent brains^{13,49} which showed that $\alpha(2-3)$ -linked Neu5Ac moieties (striatum: 8.13%, SN: 7.85%, no statistical significance) were much more abundant than that in $\alpha(2-6)$ -linked Neu5Ac glycans (striatum: 2.44%, SN: 3.11%, *p* < 0.05) (Figure 2f). In Figure 2f, we also show a regional disparity with higher levels of $\alpha(2-6)$ -linked Neu5Ac glycans in SN. We also detected the presence of phosphorylated *N*-glycans in SN (2.99%) which was not detected in the striatum. Interestingly sialic acid acetylation was detected in both the striatum (2.49%) and SN (2.20%) with no significant difference.

N-acetylneuraminic acid (Neu5Ac) and *N*-glycolylneuraminic acid (Neu5Gc) are the major sialic acids detected in most mammals. Neu5Gc is biosynthesized from Neu5Ac which acts as a sugar nucleotide donor, and cytidine monophospho-*N*-acetylneuraminic acid hydroxylase (CMAH) mediates this conversion.⁵⁰ The gene for CMAH is mutated in humans resulting in the complete absence of endogenous Neu5Gc expression throughout the body. For other mammals, there are varied ratios of Neu5Ac to Neu5Gc detected in different tissues. However, the brain stands out as an exception to this pattern where an extremely low expression of Neu5Gc is detected. In the current study, trace amounts of Neu5Gc (<3%) were detected in both the striatum and SN of the adult rat brain. This is in agreement with previous reports of minimal levels of Neu5Gc detection in mammalian brains including the rat brains.^{51,52} However, contrary to the previous reports, Ji *et al.* (2015) reported the complete absence of Neu5Gc sialylation in the mouse brain.¹⁶ The stringently conserved dichotomous expression of Neu5Gc in the rat brain and the other tissues such as liver, kidney, and so forth is suggestive of the probable adverse effects of Neu5Gc on neural development.

Another vital feature detected was the presence of densely charged structures substituted with polysialic acid (PSA). Polysialylation has been demonstrated to be a critical factor in mediating the neural cell interactions. In Figure 2f, a relatively higher fraction of polysialylation was detected in striatal *N*-glycans when compared to SN (striatum: 2.51%, SN: 1.73%, *p* < 0.01). In the present analysis, the results revealed that each glycan of this type contained one type-1 (Gal β 3GlcNAc) antenna in addition to type-2 (Gal β 4GlcNAc) chains which was found to be consistent with the studies on the polysialylated glycans of murine NCAM.⁵³ The differential expression of PSA in these regions of brain can be hypothesized to correlate with processing of sensory information and neuronal plasticity. In brain, PSA expression is correlated to the regions that exhibit physiological plasticity, suggesting that these might be related to developmental processes.⁵⁴ PSA has shown to be associated with sodium channels and NCAM in an adult rat brain.⁵⁵ In the context of Parkinson's disease, PSA-NCAM expression is induced ipsilaterally in SN of 6-OHDA parkinsonian rats which serves as a marker for reactive astrocytes which was not detectable in the striatum containing the dopaminergic terminal fields.⁵⁶ This indicates that region-specific modulation of PSA expression in the brain can be well correlated to the state of

proliferation and reactivity of the constituent cells and is usually overexpressed in the areas of high plasticity like the hypothalamo-neurohypophysial system.⁵⁷

Galactosylation. Another extensively investigated glycosylation feature of the glycoproteins is galactosylation. In the current study, there were significant differences detected between the galactosylation patterns of the striatum and SN (Figure 2g) (Tables S6 and S7). A major proportion of *N*-glycans in both the striatum (63.18%) and SN (68.15%) were agalactosylated (G0, without galactose), and a high significance was identified in the expression of agalactosylated glycans between the two regions ($p < 0.0001$). This comprised both the neutral and charged *N*-glycans. Four other classes of galactosylated *N*-glycans with one (G1, striatum: 15.45%, SN: 14.97%, no statistical significance), two (G2, striatum: 9.56%, SN: 11.53%, $p < 0.001$), three (G3, striatum: 3.24%, SN: 8.14%, $p < 0.001$), and four (G4, striatum: 4.22%, SN: 1.70%, $p < 0.001$) terminal galactose residues were also differentially regulated across the two regions of the brain. Most of these terminal galactose residues were associated with a Lewis^x or sialyl Lewis^x epitope. Previous studies correlated biantennary structures to these epitopes but contrary to these studies; however, in both striatum and SN, the biantennary structures were mainly found to be associated with one or more terminal galactose residues in both neutral and charged glycans instead.^{13,14}

Lectin Histochemistry. Lectins are the sugar-binding proteins of plant origin which can bind to the glycan moieties of several glyco-conjugates and are used for their identification.^{58,59} For fucosylation, the striatum and SN showed a differential binding profile with AAA (Figure 3a). This lectin binds to Fuc- α -(1-6) and Fuc- α -(1-3) glycan moieties. The lectin-binding profile further supports our observation of the distinct spatial distribution of fucosylated *N*-glycans with the striatum showing a more diffused, higher binding intensity than SN. Con A is known to bind to the mannose motif and shows preferential binding to oligomannose type *N*-linked glycosylation. In agreement with UPLC analysis, a higher binding intensity was observed for Con A in the SN as compared to the striatum which is indicative of a higher expression of oligomannosidic *N*-glycans (a percent volume fraction of positive staining in SN: 47.20% and striatum: 32.14%, $p < 0.001$). This further augments the region-specific distribution of oligomannosidic *N*-glycans that was observed using HILIC-UPLC and LC-MS. A region-specific distribution of WGA binding between the striatum and SN could be attributed to its strong binding affinity to the microglial cells and their processes mediated by its interaction *via N*-acetylglucosamine residues.⁶⁰ WGA strongly binds to the microglial population, and SN is densely populated by it as compared to the striatum.⁶¹ The quantified lectin histochemistry analysis is presented in Figure 3b which is in line with our UPLC analysis in this study. This presents a piece of robust evidence about the speculated correlation of the *N*-glycosylation patterns in different regions of the brain with their sub-cellular composition and biological functions.

CONCLUSIONS

This study presents the development of an elaborate glycoanalytical platform for the detailed characterization and investigation of spatial resolution of *N*-glycosylation in rodent brains. In the course of this analysis, besides achieving a detailed glycoprofile for the striatum and SN through the

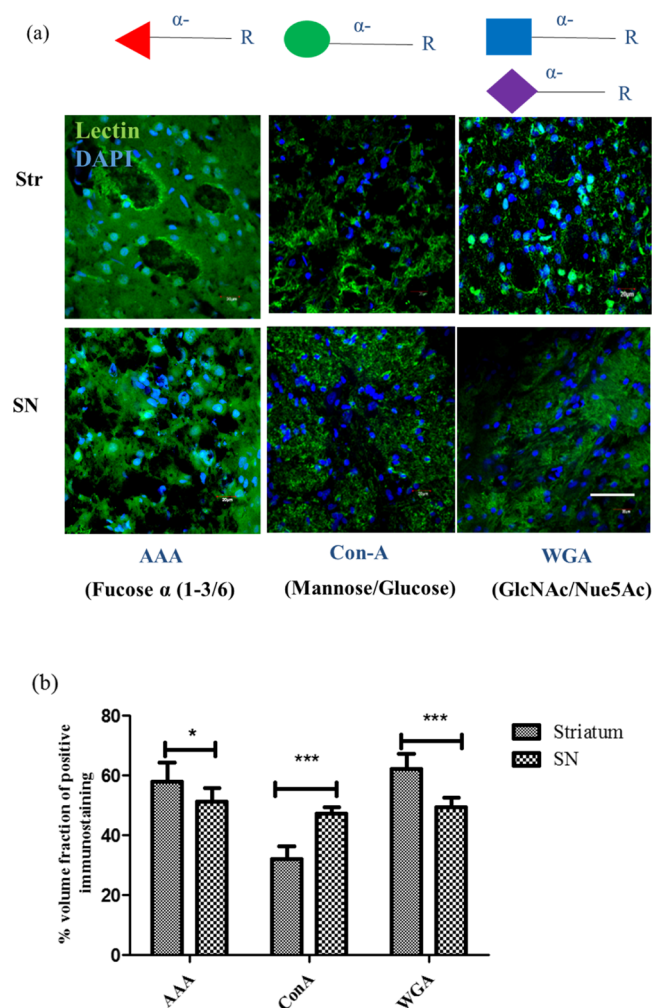


Figure 3. Lectin histochemical analysis for *N*-glycan modulation. (a) Visual representation of the differential distribution of *N*-glycans in the rat brain through the differential lectin binding profiles (green: lectin-FITC conjugates, blue: DAPI stained nuclei). Differential Con A, AAA, and WGA binding aligns with the regional resolution observed through HILIC-UPLC and LC-MS. (b) Quantified lectin histochemistry results representing the regional regulation of *N*-glycosylation in the rat brain. Data are shown as mean \pm SD for $n = 5$ animals per group, and the data were analyzed using two-way ANOVA and Bonferroni's post-hoc analysis. * and *** denotes significant differences between the different groups at $p < 0.05$ and $p < 0.001$, respectively. Scale bar = 20 μm .

identification and profiling of more than a hundred glycan structures, we were able to identify novel glycan motifs and traits. The presence of Man 6-P represents a significant trait specific to SN which was not detected as a major glycan in the striatum. Glycosylation traits such as complex and oligomannose type *N*-glycans, sialylation (mono-, di-, and tetra-), fucosylation (tri-, core and outer arm), and galactosylation (di-, tri- and tetra-), amongst others, were found to be significant between the two regions. Agalactosylation (absence of galactose, $p < 0.0001$) is another major glycosylation trait that differentiates both regions with potentially significant functional and biological implications. More importantly, this comprehensive and reproducible region-specific profiling of the brain glycome could provide significant insights and serve as a baseline for the identification of biomarkers and their regulation in neurodegenerative diseases.

■ ASSOCIATED CONTENT

SI Supporting Information

The Supporting Information is available free of charge at <https://pubs.acs.org/doi/10.1021/acs.analchem.0c01206>.

Detailed supplementary experimental procedures, additional experimental data including optimization of protein extraction protocols, reproducibility of the platform, region-specific resolution of N-glycans, using LC-MS, UPLC, exoglycosidase digestion panels, and WAX analysis for SN and striatum, individual peak area values for 26 peaks from HILIC-UPLC chromatograms for all biological replicates for both the striatum and SN, composition of their N-glycome, calculations of derived glycosylation traits, and table for significance of all calculated traits and mass spectrometric analysis of the brain N-glycans (PDF)

■ AUTHOR INFORMATION

Corresponding Author

Róisín O'Flaherty – GlycoScience Group, National Institute for Bioprocessing Research and Training (NIBRT), Co. Dublin A94X099, Ireland; orcid.org/0000-0003-1941-4775; Phone: 003531 215 8154; Email: roisin.oflaherty@nibrt.ie

Authors

Juhi Samal – CURAM-SFI Research Centre for Medical Devices, National University of Ireland, Co. Galway H91W2TY, Ireland

Radka Saldova – CURAM-SFI Research Centre for Medical Devices, National University of Ireland, Co. Galway H91W2TY, Ireland; GlycoScience Group, National Institute for Bioprocessing Research and Training (NIBRT), Co. Dublin A94X099, Ireland; UCD School of Medicine, College of Health and Agricultural Science (CHAS), University College Dublin (UCD), Co. Dublin A94X099, Ireland

Pauline M. Rudd – GlycoScience Group, National Institute for Bioprocessing Research and Training (NIBRT), Co. Dublin A94X099, Ireland; Analytics Group, Bioprocessing Technology Institute (AStar), Singapore 138668

Abhay Pandit – CURAM-SFI Research Centre for Medical Devices, National University of Ireland, Co. Galway H91W2TY, Ireland; orcid.org/0000-0002-6292-4933

Complete contact information is available at:

<https://pubs.acs.org/doi/10.1021/acs.analchem.0c01206>

Notes

The authors declare no competing financial interest.

■ ACKNOWLEDGMENTS

This project is based on the work supported by the Science Foundation Ireland (SFI) and the European Regional Development Fund (grant number 13/RC/2073) and Hardiman fellowship, NUI Galway. The authors would like to thank Maciej Doczy for his help with the graphic illustrations and Dr. Isma Liza Mohd Isa for her help with tissue collection procedures.

■ REFERENCES

- (1) Moremen, K. W.; Tiemeyer, M.; Nairn, A. V. *Nat. Rev. Mol. Cell Biol.* **2012**, *13*, 448–462.
- (2) Zhang, Y.; Yin, H.; Lu, H. *Glycoconj. J.* **2012**, *29*, 249–258.
- (3) Henion, T. R.; Faden, A. A.; Knott, T. K.; Schwarting, G. A. J. *Neurosci.* **2011**, *31*, 6576–6586.

- (4) Shur, B. D.; Roth, S. *Biochim. Biophys. Acta Rev. Biomembr.* **1975**, *415*, 473–512.
- (5) Roseman, S. *Chem. Phys. Lipids* **1970**, *5*, 270–297.
- (6) Collin, E. C.; Kilcoyne, M.; White, S. J.; Grad, S.; Alini, M.; Joshi, L.; Pandit, A. S. *Sci. Rep.* **2016**, *6*, 23062.
- (7) Haltiwanger, R. S.; Lowe, J. B. *Annu. Rev. Biochem.* **2004**, *73*, 491–537.
- (8) Szajda, S. D.; Jankowska, A.; Zwierz, K. *Dis. Markers* **2008**, *25*, 233–242.
- (9) Pučić, M.; Pinto, S.; Novokmet, M.; Knežević, A.; Gornik, O.; Polašek, O.; Vlahoviček, K.; Wang, W.; Rudd, P. M.; Wright, A. F.; Campbell, H.; Rudan, I.; Lauc, G. *Glycobiology* **2010**, *20*, 970–975.
- (10) Grünwald, S. *Biochim. Biophys. Acta (BBA) - Mol. Basis Dis.* **2009**, *1792*, 827–834.
- (11) Haeuptle, M. A.; Hennes, T. *Hum. Mutat.* **2009**, *30*, 1628–1641.
- (12) Kleene, R.; Schachner, M. *Nat. Rev. Neurosci.* **2004**, *5*, 195–208.
- (13) Zamze, S.; Harvey, D. J.; Chen, Y.-J.; Guile, G. R.; Dwek, R. A.; Wing, D. R. *Eur. J. Biochem.* **1998**, *258*, 243–270.
- (14) Chen, Y.-J.; Wing, D. R.; Guile, G. R.; Dwek, R. A.; Harvey, D. J.; Zamze, S. *Eur. J. Biochem.* **1998**, *251*, 691–703.
- (15) Wing, D. R.; Rademacher, T. W.; Field, M. C.; Dwek, R. A.; Schmitz, B.; Thor, G.; Schachner, M. *Glycoconj. J.* **1992**, *9*, 293–301.
- (16) Ji, I. J.; Hua, S.; Shin, D. H.; Seo, N.; Hwang, J. Y.; Jang, I.-S.; Kang, M.-G.; Choi, J.-S.; An, H. J. *Anal. Chem.* **2015**, *87*, 2869–2877.
- (17) Eshghi, S. T.; Yang, S.; Wang, X.; Shah, P.; Li, X.; Zhang, H. *ACS Chem. Biol.* **2014**, *9*, 2149–2156.
- (18) Raghunathan, R.; Polinski, N. K.; Klein, J. A.; Hogan, J. D.; Shao, C.; Khatri, K.; Leon, D.; McComb, M. E.; Manfredsson, F. P.; Sortwell, C. E.; Zaia, J. *Mol. Cell. Proteomics* **2018**, *17*, 1778–1787.
- (19) Stückmann, H.; O'flaherty, R.; Adamczyk, B.; Saldova, R.; Rudd, P. M. *Integr. Biol.* **2015**, *7*, 1026–1032.
- (20) Royle, L.; Radcliffe, C. M.; Dwek, R. A.; Rudd, P. M. Detailed Structural Analysis of N-Glycans Released from Glycoproteins in SDS-PAGE Gel Bands Using HPLC Combined with Exoglycosidase Array Digestions. *Glycobiology Protocols*; Humana Press: New Jersey, 2006; Vol. 347, pp 125–144.
- (21) Royle, L.; Campbell, M. P.; Radcliffe, C. M.; White, D. M.; Harvey, D. J.; Abrahams, J. L.; Kim, Y.-G.; Henry, G. W.; Shadick, N. A.; Weinblatt, M. E.; Lee, D. M.; Rudd, P. M.; Dwek, R. A. *Anal. Biochem.* **2008**, *376*, 1–12.
- (22) Küster, B.; Wheeler, S. F.; Hunter, A. P.; Dwek, R. A.; Harvey, D. J. *Anal. Biochem.* **1997**, *250*, 82–101.
- (23) Bigge, J. C.; Patel, T. P.; Bruce, J. A.; Goulding, P. N.; Charles, S. M.; Parekh, R. B. *Anal. Biochem.* **1995**, *230*, 229–238.
- (24) Saldova, R.; Kilcoyne, M.; Stückmann, H.; Martín, S.; Lewis, A. M.; Tuite, C. M. E.; Gerlach, J. Q.; Le Berre, M.; Borys, M. C.; Li, Z. J.; Abu-Absi, N. R.; Leister, K.; Joshi, L.; Rudd, P. M. *Methods* **2017**, *116*, 63–83.
- (25) Schnaar, R. L.; Suzuki, A.; Stanley, P. *Glycosphingolipids*; Cold Spring Harbor Laboratory Press, 2009.
- (26) Nakakita, S.-i.; Natsuka, S.; Okamoto, J.; Ikenaka, K.; Hase, S. J. *Biochem.* **2005**, *138*, 277–283.
- (27) Kronewitter, S. R.; de Leoz, M. L. A.; Peacock, K. S.; McBride, K. R.; An, H. J.; Miyamoto, S.; Leiserowitz, G. S.; Lebrilla, C. B. *J. Proteome Res.* **2010**, *9*, 4952–4959.
- (28) Kita, Y.; Miura, Y.; Furukawa, J.-i.; Nakano, M.; Shinohara, Y.; Ohno, M.; Takimoto, A.; Nishimura, S.-I. *Mol. Cell. Proteomics* **2007**, *6*, 1437–1445.
- (29) Dube, D. H.; Bertozzi, C. R. *Nat. Rev. Drug Discovery* **2005**, *4*, 477–488.
- (30) Everest-Dass, A. V.; Briggs, M. T.; Kaur, G.; Oehler, M. K.; Hoffmann, P.; Packer, N. H. *Mol. Cell. Proteomics* **2016**, *15*, 3003–3016.
- (31) Horstkorte, R.; Schachner, M.; Magyar, J. P.; Vorherr, T.; Schmitz, B. *J. Cell Biol.* **1993**, *121*, 1409–1421.

- (32) Jadot, M.; Lin, L.; Sleat, D. E.; Sohar, I.; Hsu, M.-S.; Pintar, J.; Dubois, F.; Coninck, S. W.-D.; Wattiaux, R.; Lobel, P. *J. Biol. Chem.* **1999**, *274*, 21104–21113.
- (33) Chiasserini, D.; Paciotti, S.; Eusebi, P.; Persichetti, E.; Tasegian, A.; Kurzawa-Akanbi, M.; Chinnery, P. F.; Morris, C. M.; Calabresi, P.; Parnetti, L.; Beccari, T. *Mol. Neurodegener.* **2015**, *10*, 15.
- (34) Nakano, M.; Mishra, S. K.; Tokoro, Y.; Sato, K.; Nakajima, K.; Yamaguchi, Y.; Taniguchi, N.; Kizuka, Y. *Mol. Cell. Proteomics* **2019**, *18*, 2044–2057.
- (35) Fogli, A.; Merle, C.; Roussel, V.; Schiffmann, R.; Ughetto, S.; Theisen, M.; Boespflug-Tanguy, O. *PLoS One* **2012**, *7*, No. e42688.
- (36) Shimizu, H.; Ochiai, K.; Ikenaka, K.; Mikoshiba, K.; Hase, S. *J. Biochem.* **1993**, *114*, 334–338.
- (37) Hua, S.; Jeong, H. N.; Dimapasoc, L. M.; Kang, I.; Han, C.; Choi, J.-S.; Lebrilla, C. B.; An, H. J. *Anal. Chem.* **2013**, *85*, 4636–4643.
- (38) Lin, S.-Y.; Chen, Y.-Y.; Fan, Y.-Y.; Lin, C.-W.; Chen, S.-T.; Wang, A. H.-J.; Khoo, K.-H. *J. Proteome Res.* **2008**, *7*, 3293–3303.
- (39) Eshghi, S. T.; Yang, W.; Hu, Y.; Shah, P.; Sun, S.; Li, X.; Zhang, H. *Sci. Rep.* **2016**, *6*, 37189.
- (40) Wetzell, W.; Popov, N.; Lössner, B.; Schulzeck, S.; Honza, R.; Matthies, H. *Pharmacol. Biochem. Behav.* **1980**, *13*, 765–771.
- (41) Fukuda, T.; Hashimoto, H.; Okayasu, N.; Kameyama, A.; Onogi, H.; Nakagawasai, O.; Nakazawa, T.; Kurosawa, T.; Hao, Y.; Isaji, T.; Tadano, T.; Narimatsu, H.; Taniguchi, N.; Gu, J. *J. Biol. Chem.* **2011**, *286*, 18434–18443.
- (42) Varki, A. *Trends Mol. Med.* **2008**, *14*, 351–360.
- (43) Chai, Q.; Arndt, J. W.; Dong, M.; Tepp, W. H.; Johnson, E. A.; Chapman, E. R.; Stevens, R. C. *Nature* **2006**, *444*, 1096–1100.
- (44) Rutishauser, U.; Acheson, A.; Hall, A.; Mann, D.; Sunshine, J. *Science* **1988**, *240*, 53–57.
- (45) Quirico-Santos, T.; Fonseca, C. O.; Lagrota-Candido, J. *Acta Neuropsychiatr. Argent.* **2010**, *68*, 799–803.
- (46) Kontou, M.; Weidemann, W.; Bork, K.; Horstkorte, R. *Biol. Chem.* **2009**, *390*, 575–579.
- (47) Wang, B. *Annu. Rev. Nutr.* **2009**, *29*, 177–222.
- (48) Rodriguez, J. A.; Piddini, E.; Hasegawa, T.; Miyagi, T.; Dotti, C. *G. J. Neurosci.* **2001**, *21*, 8387–8395.
- (49) Krusius, T.; Finne, J. *Eur. J. Biochem.* **1977**, *78*, 369–379.
- (50) Kawano, T.; Koyama, S.; Takematsu, H.; Kozutsumi, Y.; Kawasaki, H.; Kawashima, S.; Kawasaki, T.; Suzuki, A. *J. Biol. Chem.* **1995**, *270*, 16458–16463.
- (51) Davies, L. R. L.; Pearce, O. M. T.; Tessier, M. B.; Assar, S.; Smutova, V.; Pajunen, M.; Sumida, M.; Sato, C.; Kitajima, K.; Finne, J.; Gagneux, P.; Pshezhetsky, A.; Woods, R.; Varki, A. *J. Biol. Chem.* **2012**, *287*, 28917–28931.
- (52) Davies, L. R. L.; Varki, A. *Top. Curr. Chem.* **2015**, *366*, 31–54.
- (53) Geyer, H.; Bahr, U.; Liedtke, S.; Schachner, M.; Geyer, R. *Eur. J. Biochem.* **2001**, *268*, 6587–6599.
- (54) Seki, T.; Arai, Y. *Neurosci. Res.* **1993**, *17*, 265–290.
- (55) Zuber, C.; Lackie, P. M.; Catterall, W. A.; Roth, J. *Differentiation* **1994**, *57*, 119–131.
- (56) Nomura, T.; Yabe, T.; Rosenthal, E. S.; Krzan, M.; Schwartz, J. P. *J. Neurosci. Res.* **2000**, *61*, 588–596.
- (57) Kiss, J. Z.; Wang, C.; Rougon, G. *Neuroscience* **1993**, *53*, 213–221.
- (58) Collin, E. C.; Kilcoyne, M.; White, S. J.; Grad, S.; Alini, M.; Joshi, L.; Pandit, A. S. *Sci. Rep.* **2016**, *6*, 23062.
- (59) Gerlach, J. Q.; Kilcoyne, M.; Eaton, S.; Bhavanandan, V.; Joshi, L. Non-Carbohydrate-Mediated Interaction of Lectins with Plant Proteins. *Advances in Experimental Medicine and Biology*; Springer, 2011; Vol. 705, pp 257–269.
- (60) Colton, C. A.; Abel, C.; Patchett, J.; Keri, J.; Yao, J. J. *Histochem. Cytochem.* **1992**, *40*, 505–512.
- (61) Lawson, L. J.; Perry, V. H.; Dri, P.; Gordon, S. *Neuroscience* **1990**, *39*, 151–170.